Transient photocharge measurements and electron emission from deep levels in undoped *a*-Si:H

Homer Antoniadis* and E. A. Schiff
Physics Department, Syracuse University, Syracuse, New York 13244-1130
(Received 9 March 1992)

We report transient photocurrent and photocharge measurements in several undoped hydrogenated amorphous silicon (*a*-Si:H) specimens in the time domain from 10 ns to 50 s; transients were measured using coplanar electrodes between 260 and 380 K. The photocharge measurements exhibit three features which we identify with electron deep trapping, trap emission, and recombination. We analyzed the typical emission times to obtain the activation energy and frequency prefactor. The activation energy varied between 0.4 and 0.6 eV for different specimens; the frequency prefactor varied exponentially with activation energy ("Meyer-Neldel" behavior). We discuss the Meyer-Neldel dependence in terms of a temperature shift of *D*-center levels with respect to the transport edge. The emission time observations also account for the large difference between electron mobility-lifetime products estimated from time-of-flight and steady-state photocurrent measurements.

I. INTRODUCTION

In the last decade, the research of several groups has established a reasonably straightforward picture for the evolution of photogenerated electrons in undoped hydrogenated amorphous silicon (*a*-Si:H). At the earliest times electrons thermalize with exponentially distributed conduction bandtail states.[1] They are subsequently trapped by deep levels, which are usually identified with the D^0 center observed by electron-spin resonance.[2-4] Apparently, the electrons are reemitted from the traps at still later times, and after many trapping-detrapping cycles they finally recombine.[5]

Although this picture is simple, and accounts well for several aspects of photoconductivity, it cannot be considered conclusively established. In particular, the reemission stage has not been clearly observed, and its existence has been, in effect, interpolated from early and long time measurements.[6-9] The fact that a clear emission time has not been measured using transient photocurrent measurements is at least mildly surprising, since several groups have reported measurements spanning the temporal range 10^{-9}–10^{2} s.[10-21]

We have found that transient *photocharge* measurements do reveal an emission time—even when transient photocurrent measurements do not. This peculiarity obtains even for the simplest "multiple-trapping" model of photoconductivity. In this model the specimen conductivity, and hence the photocurrent, reflects only the density of mobile carriers above a band edge. After photogeneration, electrons are first trapped by a discrete level, and only recombine following emission at later times. Figure 1 shows the forms for a transient photocurrent $I(t)$ and the transient photocharge $Q(t)$ following a short photogeneration impulse calculated analytically using this model. The mathematical details have been published elsewhere.[5,22,23] The photocurrent transient clearly shows trapping at time t_T. Before t_T all photocarriers contribute to the photocurrent, whereas following t_T only the relatively small density of mobile carriers established by the competition of trapping and reemission contribute to the current. The recombination response time t_R is also indicated, but the feature we wish to emphasize is that the trap emission time (denoted t_E in the figure) is not apparent. This point has been emphasized by Marshall and Main,[22] who explained that a Boltzmann distribution of carriers between the conduction band and the trap is established at t_T, and that there is no thermali-

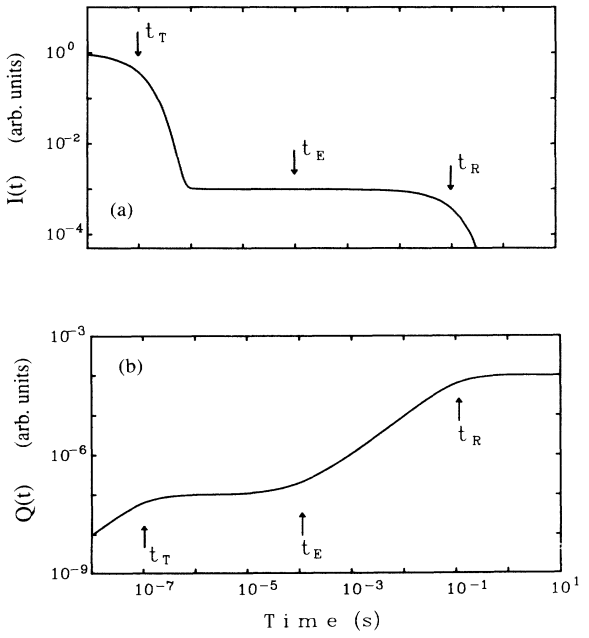

FIG. 1. (a) Transient photocurrent $I(t)$ and (b) transient photocharge $Q(t)$ corresponding to the monoenergetic trap model discussed in the text. We indicate with arrows the characteristic deep-trapping time t_T, emission time t_E, and recombination response time t_R.

zation feature at the emission time.

The simple expedient of integrating $I(t)$ to obtain the photocharge $Q(t)$ reveals the emission time clearly enough for this model. The photocharge is proportional to the time-integrated density of mobile photocarriers. The value of $Q(t)$ reached by t_T is proportional to the product of the total density of photocarriers and the mean trapping time. In order to double the value of $Q(t)$ one must wait for the emission time, so that a carrier typically undergoes two trapping cycles. The large gap between t_T and t_E explains the broad plateau in $Q(t)$ and the clear delineation of t_E.

Although defects in a-Si:H are better described by a distribution of trap emission times than by the single time in this model, the photocurrent and photocharge measurements we have made appear to show features which are qualitatively similar. In Fig. 2 we have presented some of our transient photocurrent and photocharge data taken using "gap cell" or coplanar electrodes. The measurements reflect the motion of electrons; additional experimental details will be presented subsequently. A careful inspection of the $Q(t)$ measurements appears to reveal an emission time feature; we encourage the reader to examine the measurements by placing her (or his) eyes (and head) next to the page.

We have also examined models for transient photocurrents and photocharges using a spread of trap depths and emission times. This refinement accounts for the most apparent difference between the model of Fig. 1 and the data of Fig. 2, which is the subunity power law describing the increase of the photocharge following t_E in the a-Si:H measurements. The model with a single trap level yields a linear rise of $Q(t)$ following emission. We attribute this aspect to exponential tails around the peak energy of the defect level; the energy parameter of the exponential is about 50 meV, corresponding to a width of the energy distribution of about 0.15 eV. Some approximate analytical calculations have been reported previously;[20,24] essentially exact numerical simulations will be published elsewhere.[25]

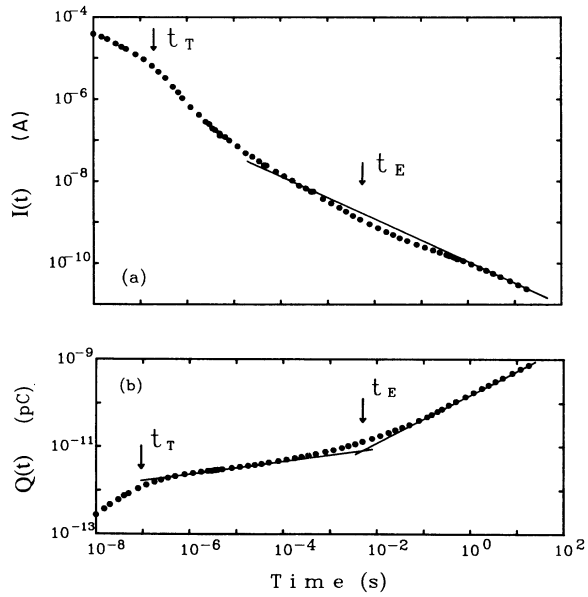

FIG. 2. (a) Transient photocurrent $I(t)$ and (b) transient photocharge $Q(t)$ corresponding to an a-Si:H specimen at room temperature. We indicate with arrows the characteristic deep-trapping time t_T and the emission time t_E. The emission time t_E is taken to be the time given by the intersection of the two lines illustrated.

In this paper we present temperature-dependent, transient photocharge measurements for several specimens of undoped a-Si:H. We found that a single photocharge transient—spanning the time range between 10 ns and 50 s—exhibits the complete sequence of transport events: band transport, deep trapping, subsequent thermal emission of deep-trapped carriers, and then finally recombination.

We have estimated the activation energy and the frequency prefactor ν_0 associated with the emission time feature; we attribute these to the properties of defects near the peak of the trap energy distribution. We concluded that this trap distribution in a-Si:H is not a monolithic entity, but varies significantly between specimens. For the four specimens reported here the activation energy varied between 0.4 and 0.6 eV. Additionally, the prefactor showed an exponential "Meyer-Neldel" dependence upon the activation energy.[26,27] To explain this behavior we suggest a mechanism of temperature dependence of the energy of the trap with respect to the mobility edge.

We also consider these emission time measurements to be important in a second context, which is the interpretation of mobility-lifetime product estimates in undoped a-Si:H. In particular there is about two orders of magnitude difference between the electron deep-trapping mobility-lifetime product estimated from charge-collection experiments, and the steady-state mobility-lifetime product derived from steady-state photoconductivity.[6,28] For the measurements reported here we are able to show conclusively that this effect is due entirely to the different time scales of the charge-collection and steady-state measurements, and thereby exclude several other proposed mechanisms for it.[6,29–32]

This paper is organized as follows. In Sec. II we give an introduction to mobility-lifetime products and their relationship to photocurrent and photocharge measurements. In Sec. III we describe the specimens and the experimental methods used for the transient photocharge measurements. In Sec. IV we present our experimental results on transient photocharges for several specimens of varying defect densities. In Sec. V we present our analysis of the photocharge transients in terms of a trap emission time; from the temperature dependence we estimate the mean depth of the deep trap and an associated frequency prefactor ν_0. We also report a Meyer-Neldel relation which is found to exist between the prefactor frequency and the mean depth of the trap. In Sec. VI we present our experimental estimates of mobility-lifetime products from transient photocharge measurements and from steady-state photoconductivity experiments. Finally in Sec. VII we briefly discuss possible scenarios for the evolution of holes in a-Si:H.

II. MOBILITY-LIFETIME PRODUCTS UNDER TRANSIENT AND STEADY-STATE CONDITIONS

In a transient photocharge experiment the transient photocharge $Q(t)$ collected in the external circuit at time t after photogeneration provides an estimate of the average distance $x(t)$ the photocarriers have drifted since photogeneration. A simple expression is obtained when the energy supplies by the external bias is equated with the work done by a uniform electric field E in moving the mean position of the total photocarrier charge Q_0 a distance $x(t)$:

$$Q(t)V=Q_0x(t)E \ . \tag{1}$$

Taking $E=V/d$, where d is the spacing between the electrodes, we obtain

$$\frac{x(t)}{d}=\frac{Q(t)}{Q_0} \ . \tag{2}$$

Assuming that the displacement $x(t)$ is proportional to E, we define the ratio $x(t)/E$ as the *displacibility*

$$\zeta(t)\equiv\frac{x(t)}{E} \ . \tag{3}$$

Expressing $\zeta(t)$ in terms of the measured photocharge $Q(t)$ we obtain

$$\zeta(t)=Q(t)\frac{d}{Q_0E}=Q(t)\frac{d^2}{Q_0V} \ . \tag{4}$$

The transient photocharge measurements presented in this paper will be normalized by multiplying by d^2/Q_0V; the product has the dimensions of a mobility-lifetime product $\mu\tau$. This normalization is obviously a convenient way to avoid trivial dependences upon interelectrode distance d, electric field E, and total photocarrier charge Q_0. Additionally, $\zeta(t)=Q(t)(d^2/Q_0V)$ is closely related to both mobility-lifetime products commonly reported in *a*-Si:H. First, $Q(t)(d^2/Q_0V)$ evaluated at 10 μs is completely equivalent to the deep-trapping mobility-lifetime product measured using the "charge-collection" technique (using the conventional 10-μs integration time); this equivalence is expected analytically, and is confirmed by experimental comparison of the two views.[3,13,33–35] Second, we can show that $\zeta(\infty)$ is equivalent to a steady-state mobility-lifetime product $\mu\tau_{ss}$.

The standard definition of $\mu\tau_{ss}$ is $\sigma_{ph}=eG\mu\tau_{ss}$,[5] where σ_{ph} is the photoconductivity, e the electronic charge, and G the volume photogeneration rate. A short calculation permits this equation to be recast into a somewhat more general form:

$$\mu\tau_{ss}=i_{ss}\frac{d^2}{i_0V} \ . \tag{5}$$

Here i_{ss} is the steady-state photocurrent measured in the bias circuit. i_0 is the "photogeneration current" (the charge photogenerated throughout the structure per unit time), which for homogeneous illumination is the product $eGAl$, where A is the illuminated area and l the sample thickness. Notice the similarity of Eq. (4) with (5): the steady-state mobility-lifetime product $\mu\tau_{ss}$ characterizes the response of the specimen to a steady-state generation current "i_0," while the displacibility $\zeta(t)$ will be related to the charge response of the specimen to a single photogeneration pulse "Q_0." A short calculation given elsewhere[5,6] shows that $\mu\tau_{ss}$ can be identified with $\zeta(\infty)$ when photocurrents depend linearly upon photogeneration.

III. SPECIMENS AND EXPERIMENTAL METHODS

Hydrogenated amorphous silicon *a*-Si:H specimens were deposited at Syracuse University using a commercial (Plasma Technology, Inc. "Plasmalab") 13.56-MHz rf plasma reactor operating with 200 mT of pure silane gas at 5 W of rf power. Specimens where deposited onto Corning 7059 glass substrates; substrate temperatures were varied from 150 to 350 °C. The densities of paramagnetic dangling centers were measured using electron spin-resonance spectroscopy.[4] The specimen properties are collected in Table I.

Standard *wide-gap coplanar* contacts were evaporated onto the *a*-Si:H film following deposition. The gap between the electrodes was 500 μm. Aluminum was used for the low defect specimens and chromium for more defective ones.

The electrode structure was illuminated by a pulsed (3-ns) nitrogen-laser pumped dye laser (Laser Science, Inc.). Wavelengths between 590 and 620 nm were used; for these wavelengths the typical absorption lengths range from 0.1 to 0.5 μm.[20] The laser intensity incident upon the specimen was calibrated using an auxiliary crystalline silicon *p-i-n* diode and the manufacturer's specifications.

Transient photocurrent and photocharge measurements were performed using an apparatus shown

TABLE I. Properties of the specimens: T_s is the substrate deposition temperature, d is the thickness of the specimens, N_S is the density of spins measured with ESR, and $\mu\tau_{e,t}$ is the electron deep-trapping mobility-lifetime product. $\mu\tau_{ss}$ is the electron steady-state mobility-lifetime product estimated from steady-state photoconductivity under illumination $F=2\times10^{11}$ photons/cm^2 s. $\mu\tau_{e,t}$ and $\mu\tau_{ss}$ have been estimated at room temperature. Specimen number 5 was deposited originally at 150 °C then annealed at 225 °C for 1 h and 30 min and finally quenched at room temperature. The above specimens numbers 1, 2, 3, 4, 5, 6 have also appeared under the coding NOVAN, 314LS, 413AN, 46AN, 150TR, 200C, respectively in Ref. 35.

Specimen	T_s (°C)	d (μm)	N_S (spins/cm^3)	$\mu\tau_{e,t}$ (cm^2/V)	$\mu\tau_{ss}$ (cm^2/V)
1	250	3.3	$\sim3\times10^{15}$	2.3×10^{-7}	2.9×10^{-5}
2	350	2.0	1.4×10^{16}	5.2×10^{-8}	1.4×10^{-5}
3	195	1.5	1.2×10^{17}	6.9×10^{-9}	6.1×10^{-7}
4	160	0.9	3.9×10^{17}	6.8×10^{-10}	3.1×10^{-8}
5	225	2.1		1.7×10^{-8}	3.2×10^{-6}
6	200	2.4		1.2×10^{-7}	9.7×10^{-6}

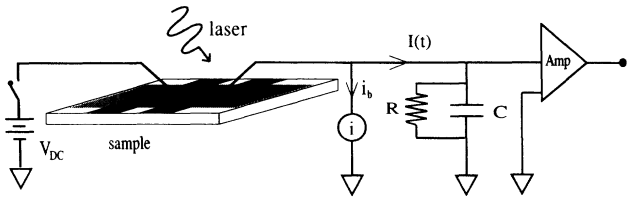

FIG. 3. Schematics for the transient photocharge measurements. The geometry of the substrate (Corning 7059) and of the coplanar electrodes evaporated onto the *a*-Si:H are shown. V_{DC} is the externally dc applied voltage; $I(t)$ is the transient photocurrent; i_b is the opposing steady-state current; C and R are the input capacitor and resistance, respectively.

schematically in Fig. 3. The amplifier output was recorded using a digital oscilloscope (LeCroy, Inc. model 9400) and downloaded to a computer. The laser intensity fluctuated about 15–20% between pulses; we averaged between 20 and 200 transients to obtain our reported results.

For times $t \ll RC$ the system records the photocharge transient; for $t \gg RC$ the system records a photocurrent. We varied R, C, the particular amplifier, and the amplifier's frequency filter settings depending upon the type of measurement (photocurrent or photocharge) and the desired time domain.

We reduced the incident laser intensity until photocharge or photocurrent responses were linear in intensity; the photon flux incident upon the specimen was typically less than 10^{12} photons/cm^2 in each pulse. We also verified that the laser repetition rate was sufficiently low not to affect transient measurements to within our nominal reproducibility of 5–10%; the acceptable rate varied according to the particular delay time, specimen, and temperature. During the photocharge measurement the specimen was kept in the dark to avoid optical bias effects[12,17] from accidental room light illumination.

We used a dc voltage bias; photocurrents and photovoltages were linear with the voltage for all results presented here. We have developed techniques based upon displacement charge measurements in response to voltage steps to diagnose whether significant space charge was stored in electrode regions of the specimen under voltage bias; the measurements are reported elsewhere.[36] When this excess space charge was negligible compared to the charge expected simply from the geometrical capacitance (the product CV), the photocharge was proportional to the bias voltage. When the excess space charge was comparable to the geometrical charge the photocharge measurements were seriously non-Ohmic. We conclude that the electric field between the electrodes was V/d to within 10% or better for the reported measurements.

For photocharge measurements for very long times and at higher temperatures the accumulation of charge upon the integrating capacitor due to the dark currents in the specimen were significant. We circumvented this difficulty by sinking the dark current into a constant current source i_b (cf. Fig. 3).

IV. TRANSIENT PHOTOCHARGE MEASUREMENTS

A. Spin-density dependence

In Fig. 4 the normalized transient photocharge $Q(t)(d^2/Q_0V)$ is plotted for four *a*-Si:H specimens of widely varying spin density in the time range between 10 ns and 45 s. The measurements were at room temperature. The total photocarrier charge Q_0 was estimated from the incident laser intensity and a correction for the specimen's reflectivity; absorption of the laser was essentially complete, and we assumed the quantum efficiency for photocarrier generation to be close to unity.[37]

The specimen number 1 (cf. Table I) is a low defect density material. The specimen number 2 is a low defect material similar to the above but it has been light soaked for two hours under 300 mW/cm^2 of white light illumination (type *ENH* halogen-tungsten bulb). The two lower curves (specimens 3 and 4) correspond to specimens deposited under suboptimal deposition conditions.

We interpret these data as estimates of the ratio of the drift of a photocarrier and the electric field $x(t)/E$ [cf. Eqs. (3) and (4)]; for convenience we refer to the ratio $x(t)/E$ as a displacibility $\zeta(t)$. We attribute this drift entirely to electron motion; as we show subsequently, this attribution is consistent with other measurements of electron drift.[35,38]

The time dependence of $Q(t)(d^2/Q_0V)$ can be readily interpreted using the stages of electron photocarrier evolution described in the introduction. The approximately linear rise at early times for the two best specimens corresponds to the bandtail multiple-trapping regime. In this regime we have $\mu \sim [x(t)/E]/t = Q(t)(d^2/Q_0V)/t$. We estimate an electron drift mobility of about 0.5 cm^2/Vs for both specimens. This value agrees with standard time-of-flight measurements on electrons in *a*-Si:H.[1,39] For the two poorer specimens we are unable to estimate the bandtail drift mobility. We cannot exclude series resistance effects as an explanation for the early time features ($t \sim 10^{-8}$ s) for these latter two specimens; photocharge measurements with an integrating capacitor are somewhat more sensitive to these effects than standard photocurrent measurements using a 50-Ω impedance amplifier.

The first stage is terminated at a broad plateau as indicated by the arrows labeled t_T; electrons are "deep trapped" at about t_T. Note that t_T occurs at earlier times for specimens with increasing spin density, consistent with the assignment of t_T to deep trapping. For example, t_T for the best quality specimen is around 600 ns while for the worst specimen it has been reduced to less than 10 ns.

Following deep trapping the photocarriers are relatively immobile and further increase in $Q(t)(d^2/Q_0V)$ is not significant until the "kink" labeled t_E. We show below that t_E is thermally activated, as anticipated for an emission time.[5]

It is instructive to calculate the actual drift of the electrons represented in Fig. 4. The field was 100 V/cm for the uppermost curve; for $Q(t)(d^2/Q_0V) = 10^{-4}$ cm^2 V we

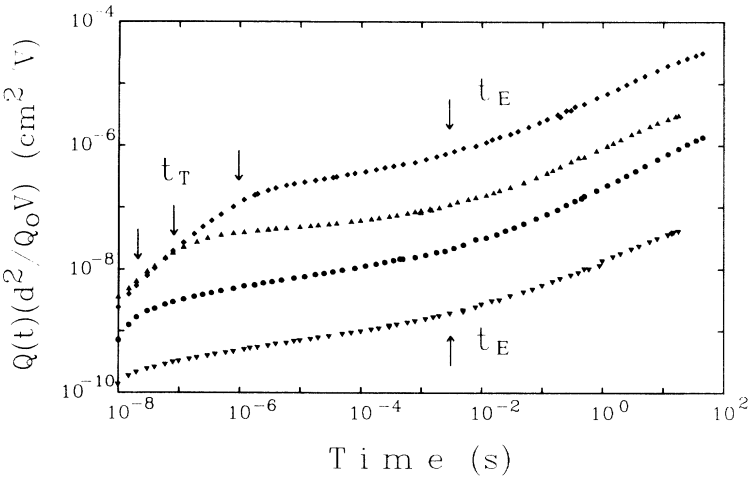

FIG. 4. Normalized transient photocharge $Q(t)(d^2/Q_0V)$ at room temperature for four different a-Si:H specimens having defect densities varying between 3×10^{15} to 3×10^{17} spins/cm^3 (the symbols ◆, ▲, ●, and ▼ correspond to specimens 1, 2, 3, and 4, respectively, in Table I). We indicate the emission times with arrows. The deep-trapping times for the top three specimens are also indicated.

estimate $x=10^{-2}$ cm, which is somewhat less than the electrode gap. For the poorer specimens drift was much less. We can summarize these remarks by the statement that the photoconductive gain in our measurements was *less* than one.

The electron deep-trapping mobility-lifetime product $\mu\tau_{e,t}$ usually measured using the "charge-collection" procedure in standard time-of-flight specimens[3,13,33–35] can also be obtained from $Q(t)(d^2/Q_0V)$ measurements such as those of Fig. 4. In particular $Q(t)(d^2/Q_0V)$ evaluated at 10 μs is nearly identical with estimates of $\mu\tau_{e,t}$ obtained by charge collection with a 10-μs integration time.[35]

In Fig. 5 we illustrate the correlation of $\mu\tau_{e,t}$ obtained from our $Q(t)(d^2/Q_0V)$ measurements with the spin density N_S; the results are an extension of an earlier report from our laboratory.[4] They broadly support the identification of deep trapping with electron capture by

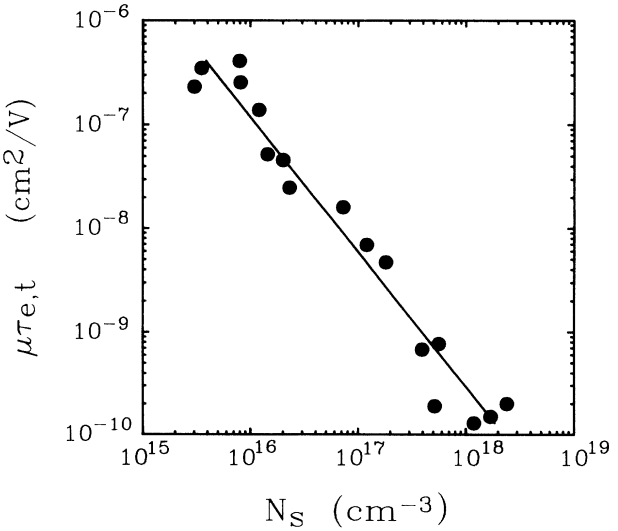

FIG. 5. Correlation of electron deep-trapping mobility-lifetime product $\mu\tau_{e,t}$ and spin defect density N_S for a variety of a-Si:H specimens having defect densities between 3×10^{15} to 3×10^{18} spins/cm^3. Deviations from the relation $\mu\tau_{e,t}=\mu_0/b_tN_S$ (Refs. 2 and 4) are obvious in the graph. The line shown is the best fit to the data.

the D.[0,2–4,13,40] However, the scatter of these data exceeds our estimates of the experimental reproducibility, which suggests that the spin density is not the only specimen parameter determining $\mu\tau_t$. The best-fit power law to these data is $\mu\tau_{e,t}\propto N_S^{-1/3}$. This dependence is slightly stronger than expected for the simplest model

$$\mu\tau_{e,t}=\frac{\mu_0}{b_tN_S}\ , \tag{6}$$

where the fundamental mobility μ_0 and the trapping parameter b_t would presumably be independent of N_S. For the lower spin densities of Fig. 5 the value of b_t/μ_0 is about 10^{-9} V cm. As we shall show shortly, we have evidence that the emission times characteristic of these traps in undoped a-Si:H do vary between specimens. It is thus certainly reasonable to speculate that the capture parameter b_t might also vary somewhat without challenging the suggestion that the trap be identified with the D center.

B. Temperature dependence

In this section we present the temperature dependence of $Q(t)(d^2/Q_0V)$ for two specimens. In Fig. 6(a) we present $Q(t)(d^2/Q_0V)$ for the specimen number 3 (cf. Table I) between 260 and 377 K. The emission times t_E, indicated with arrows, show a strong temperature dependence which will be analyzed in more detail in the next section. For the 377-K transient we see a second plateau at late times $t\sim1$ s. This plateau is a new feature which was not apparent in our time range of room temperature. We establish in Sec. VI B that the value of $Q(t)(d^2/Q_0V)$ for this second plateau can be identified with the high-temperature *recombination* mobility-lifetime product $\mu\tau_{e,r}$.

In Fig. 6(b) we show the $Q(t)(d^2/Q_0V)$ for the specimen number 2 (cf. Table I) for two temperatures 295 and 357 K; the general features are similar to those for the specimen number 3.

V. EMISSION TIMES

A. Observations

Detailed temperature dependence of the transient photocharge was performed for four specimens deposited at different deposition conditions (cf. Table I); some of these

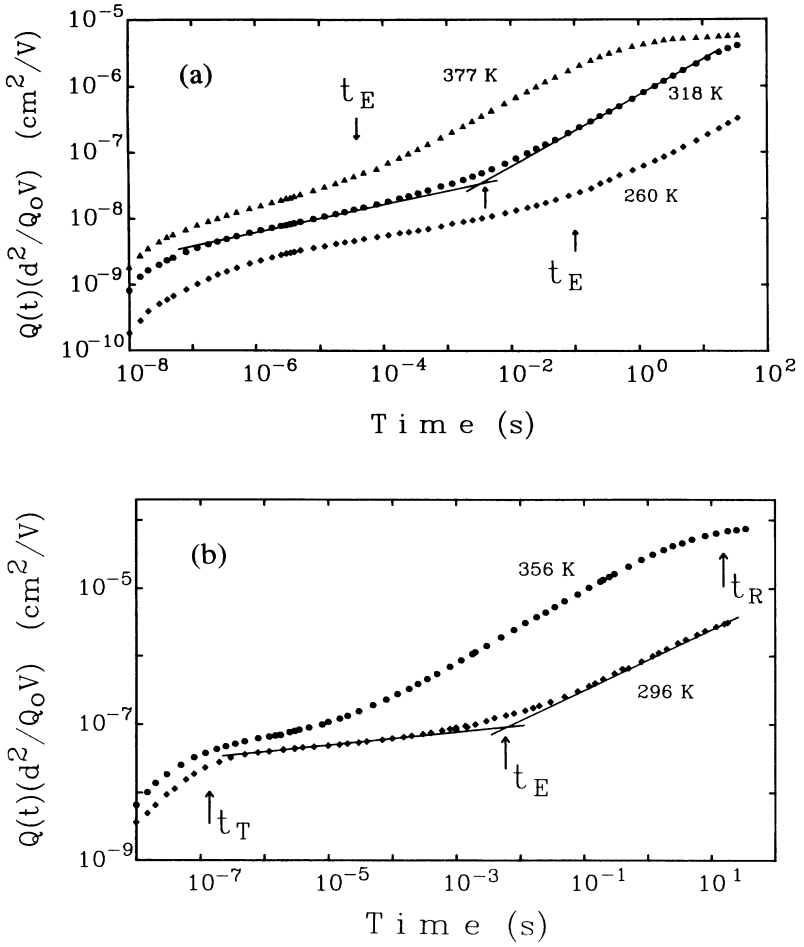

FIG. 6. Temperature dependence of the normalized transient photocharge $Q(t)(d^2/Q_0V)$ for two specimens. The top graph (a) is for specimen 3 ($N_S=1.2\times10^{17}$ spins/cm^3, cf. Tables I and II). The bottom graph (b) is for specimen 2 ($N_S=1.4\times10^{16}$ spins/cm^3, cf. Tables I and II). The arrows indicate the emission time estimates. The trapping time t_T is also indicated in the second graph.

measurements were presented in Fig. 6. From these measurements we estimated an emission time t_E for each temperature. We have not found an entirely satisfactory procedure for estimating t_E; in practice, we fitted a power law to data above and below the emission time kink, and used the intersection point to estimate t_E. The procedure is illustrated in Fig. 6.

In Fig. 7 we have graphed the inverse of the emission time $1/t_E$ as a function of the reciprocal temperature $1000/T$ for these specimens. Note that the data for each specimen are displaced by factors of 10 to prevent overlap. The straight lines drawn through these data are fits to the form

$$\frac{1}{t_E}=\nu_0\exp\left[-\frac{E_A}{k_BT}\right], \tag{7}$$

where ν_0 is a frequency prefactor, E_A the activation energy, and k_B the Boltzmann constant. The parameters E_A and ν_0 assigned to each specimen are shown in Table II, and in Fig. 8 we show the correlation of these two parameters. The correlation suggests a *Meyer-Neldel relation* (MNR) (Refs. 26 and 27) between E_A and ν_0:

$$\nu_0=\nu_{00}\exp\left[\frac{E_A}{E_{\rm MN}}\right], \tag{8}$$

where $E_{\rm MN}=26$ meV will be the energy factor of the

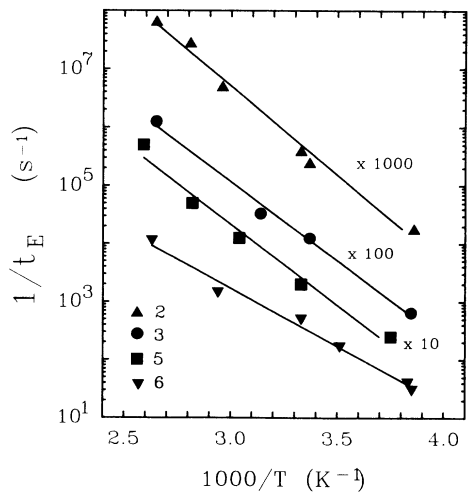

FIG. 7. Thermal emission rate $1/t_E$ versus $1000/T$ for the specimens 2, 3, 5, 6. The four sets of data are displaced from each other for clarity. The straight lines shown are the best fits to the data. The corresponding activation energies E_A as well as the frequency prefactors ν_0 are shown in Table II.

TABLE II. Summary of temperature-dependence measurements: E_A is the activation energy of the emission time t_E, ν_0 is the frequency prefactor, E_{dark} is the activation energy of the dark current. See text for γ and $\nu_{\max}$.

Specimen	E_A (eV)	ν_0 (Hz)	γ ($\times 10^{-4}$ eV/K)	E_{dark} (eV)	$\nu_{\max}$ (Hz)
2▲	0.60	6.6×10^{12}	1.6	0.70	1.6×10^{9}
3●	0.54	1.6×10^{11}	−1.6	0.80	8.2×10^{10}
5■	0.55	4.7×10^{11}	−0.7	0.75	1.5×10^{10}
6▼	0.39	1.6×10^{9}	−5.5	0.75	1.5×10^{10}

Meyer-Neldel relation and ν_{00} a MNR prefactor. The scatter of the data around the proposed Meyer-Neldel line is comparable to the errors in estimating E_A and ν_0 using the linear regression lines of Fig. 7. We discuss this interesting effect in the following section.

B. Discussion

The deep-trapping and emission data just presented establish the existence of an electron level 0.4–0.6 eV below the transport energy in *a*-Si:H; we assume that the activation energy for the emission time estimates the median level depth, based on the model for emission from a trap

$$\frac{1}{t_E}=\nu\exp\left[\frac{-(E_C-E_D)}{k_BT}\right], \tag{9}$$

where ν is the attempt-to-escape frequency, E_C is the energy of the conduction-band transport edge, and E_D is the energy of the deep level. Our measurements suggest that the properties of the deep level in *a*-Si:H vary between specimens. Despite this variability, it seems most likely to us that the deep level involved is the *D* center observed by electron spin resonance (ESR); we base this statement on the fair correlation of $\mu\tau_{e,t}$ with N_S and also on the fact that only the signature of the *D* center was observed in our specimens by ESR under the measurement conditions.

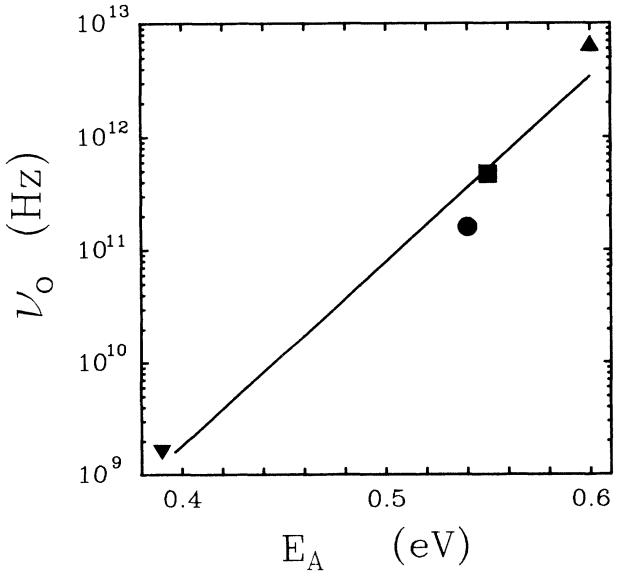

FIG. 8. Correlation of the frequency prefactor and the activation energy E_A, a Meyer-Neldel type relation is obvious from the graph. Symbols are same as for Fig. 7.

We do not have a clear understanding of which deposition parameters and specimen treatments affect E_A. The typical emission times and activation energies we have reported appear to be consistent with recent measurements in undoped *a*-Si:H based upon the modulated photocurrent technique.[41–43] This congruence is not surprising; modulated photocurrent measurements as a function of frequency are related by Fourier transformation to transient photocurrent and photocharge measurements.[25,44,45] We are unaware of other measurements which clearly show the emission process, although there are numerous estimates of the trap depth based on modeling of other experiments.[46–52] We note that Leen and Cohen[52] have recently reported measurements suggesting that this activation energy may be independent upon the time scale of the measurements due to slow atomic configuration changes in the deep level.

In addition, we have reported a Meyer-Neldel type correlation between this activation energy and the frequency prefactor ν_0. We shall discuss models relating ν_0 to the attempt-to-escape frequency ν for emission shortly. For *a*-Si:H, Meyer-Neldel relations (MNR) (Ref. 26) have previously been reported for dark electrical conductivity, thermopower, field-effect conductance, and space-charge-limited current,[27] as well as for annealing of metastable defects[53] and diffusion of hydrogen.[54,55] The occurrence of a MNR for electronic emission times has not to our knowledge been reported previously for *a*-Si:H.

There are two principal views of Meyer-Neldel type correlations. The first is literal: differences in activation energy are in fact correlated with differences in the attempt-to-escape frequencies revealed by the Meyer-Neldel correlation. This effect is well established for capture by deep, neutral traps in crystalline silicon.[56] Such a dependence can be rationalized in terms of the multiphonon emission processes required for a carrier to be captured by a trap.[57–59] The second view of Meyer-Neldel relations is that the variation in ν_0 is ultimately caused by temperature-dependent trap depths; the "true" attempt-to-escape frequency ν is temperature and trap depth independent. Of course both mechanisms may be involved for a specific defect system.

We believe that the literal view—that the microscopic attempt-to-escape frequency ν varies by more than three decades—is unlikely. Large variations in ν should give comparable variations in the trapping coefficient b_t. It is commonly assumed that the two parameters are related by a detailed balance relation $\nu=N_Cb_t$, where N_C is an effective conduction-band density of states. Accepting that the large variation in ν is microscopically correct would invalidate the straightforward interpretation of the correlation between $\mu\tau_{e,t}$ and N_S in Fig. 7:

$$\mu\tau_{e,t}=\frac{\mu_0}{b_tN_S}=\frac{\mu_0N_C}{\nu N_S}. \tag{10}$$

On the other hand, even if the straightforward interpretation of the $\mu\tau_{e,t}$-N_S correlation is accepted, both the scatter and the trend of Fig. 5 suggest that the capture

coefficient b_t varied slightly between specimens.

The interpretation of Meyer-Neldel relations based on thermal shifts of band edges and defect levels works as follows. We assume that the relative position of the deep-trap level with respect to the conduction-band edge $\Delta E_D(T)=E_C(T)-E_D(T)$ depends upon the temperature[27,60] according to the following empirical relation:

$$\Delta E_D(T)\cong\Delta E_D(0)-\gamma T\ , \tag{11}$$

where γ is a coefficient describing the temperature shift of band edge and band gap[61–65] and $\Delta E_D(0)$ the value of ΔE_D extrapolated to $T=0$. Substituting this relationship into the expression for the emission time [Eq. (9) above], we obtain

$$\frac{1}{t_E}=\nu\exp\left[-\frac{\Delta E_D(T)}{k_BT}\right] \tag{12}$$

$$=\nu\exp\left[\frac{\gamma}{k_B}\right]\exp\left[-\frac{\Delta E_D(0)}{k_BT}\right]\ . \tag{13}$$

The frequency prefactor ν_0 is thus related to ν and γ as

$$\nu_0=\nu\exp\left[\frac{\gamma}{k_B}\right]\ . \tag{14}$$

The measured activation energy E_A is equal to $\Delta E_D(0)$.

If we accept this second view of ν_0, then we can estimate a value for the coefficient γ required to account for the difference between the prefactor ν_0 and some nominal attempt-to-escape frequency ν which remains constant between specimens. Assuming $\nu=10^{12}$ Hz for the microscopic attempt-to-escape frequency we can estimate the different values of γ from

$$\gamma=k_B\ln\frac{\nu_0}{\nu}\ . \tag{15}$$

The suggested values for γ are collected in Table II. The largest value of γ is 5.5×10^{-4} eV/K. This estimate is consistent with thermal shifts of the electron mobility edge measured using internal photoemission, which yielded the range 2×10^{-4} to 8×10^{-4} eV/K.[61–63] A similar magnitude is also reported for the temperature dependence of the optical band gap.[64,65] It seems clear that thermal shifts are sufficiently large to account for most of the observed variation in ν_0.

There is nonetheless two troubling features to these interpretations. First, it seems quite surprising that the parameter b_t describing trapping should be fairly constant when the trap binding energy E_C-E_D and its temperature dependence vary significantly between the four specimens. We are unaware of any similar behavior for crystalline defect systems; for crystalline silicon, substantial changes in b_t are associated with changes in deep level binding energies.[56]

The second troublesome feature is that the conventional value of $\nu\sim10^{12}$ Hz noted above predicts a feature to our photocharge transients which we did not observe. In particular, prior to recombination in the high-temperature transients we expected to observe "complete thermalization" of the photocarrier distribution; we are implicitly assuming that the photocarriers are thermalizing in a continuous density of states extending to the dark Fermi energy. Complete thermalization then occurs for times greater than the time t_{sat} for a carrier to be emitted from a trap at the dark Fermi level:

$$t_{sat}=\frac{1}{\nu}\exp\left[\frac{E_C-E_F}{k_BT}\right]\ . \tag{16}$$

Following t_{sat} transport would be nondispersive [i.e., the relationship between $Q(t)$ and t should be linear]. A similar argument was given earlier by Pandya and Schiff[17] regarding the effects of quasi-Fermi levels on photocurrent transients.

We used the absence of this phenomenon to estimate an upper limit to ν for each specimen. We used the observed value of the recombination response time t_R as a lower bound to t_{sat}. We used the activation energy of the dark current E_{dark} to estimate E_C-E_F. Using this procedure and Eq. (16) above we calculated the values listed at ν_{max} in Table II; note that ν_{max} is about 10^9 Hz in one case. The procedure neglects the temperature dependence of E_C-E_F; including an estimate of the temperature dependence of E_C-E_F led to even smaller values for ν_{max}. Such low values seem completely incompatible with the detailed balance principle $\nu=N_Cb_t$ if we use the value $b_t\sim10^{-8}$ cm^3/s suggested by Fig. 5 and the conventional value $N_C\sim10^{19}$ cm^{-3}.

We have been unable to fully resolve these interpretive difficulties. Extensions of the analysis to incorporate defect relaxation effects seem to hold some promise for resolving them, but we shall not attempt this here.

VI. MOBILITY-LIFETIME PRODUCTS

As we have seen in Sec. II, transient photocharge $Q(t)$ measurements give estimates of a displacibility $\zeta(t)=Q(t)(d^2/Q_0V)$ [cf. Eq. (4)]. In this section we present additional measurements supporting the identity of mobility-lifetime products estimated by transient photocharge or by steady-state photocurrents. We also present the correlation of steady-state mobility-lifetime product $\mu\tau_{ss}$ and electron deep-trapping mobility-lifetime product $\mu\tau_{e,t}$ measurements for a wide range of specimens and light-soaking states; these data confirm the well-known empirical relation $\mu\tau_{ss}=100\times\mu\tau_{e,t}$ (Refs. 6 and 28) over nearly four orders of magnitude. We then briefly discuss our interpretation of the various $\mu\tau$ products for electrons in a-Si:H.

A. Evaluation of $\mu\tau_{ss}$ and $\mu\tau_{e,t}$

We performed quasi-steady-state photocurrent experiments by operating the pulsed laser at 20 Hz and recording the time-averaged photocurrent; we found that the photocurrent did not decay significantly under our measurement conditions between pulses. This technique permitted us to measure steady-state $\mu\tau$ products with exactly the same wavelength of light used in the transient photocharge measurements.

The steady-state value $\mu\tau_{ss}$ was estimated from the expression $\mu\tau_{ss}=i_{ss}(d^2/i_0V)$ [cf. Eq. (5)], where i_{ss} is the average (steady-state) photocurrent, V is the bias voltage, and d is the interelectrode gap. The photogeneration current i_0 (the charge generation in the sample volume

per unit time) was estimated from measurements of the average laser intensity (using a *c*-Si *p-i-n* diode) and from the specimen dimensions and optical-absorption properties. The procedure is nearly identical to that used to obtain Q_0 for the transient photocharge measurements [cf. Eq. (1)].

At sufficiently high temperatures we were able to estimate a recombination mobility-lifetime product from the value of $Q(t)(d^2/Q_0V)$ at 10 s, which was longer than the recombination response time t_R [see Figs. 6(a) and 6(b)]. We denote this value $\mu\tau_{e,r}$. In Fig. 9 we have graphed $\mu\tau_{ss}$ and $\mu\tau_{e,r}$ at $T=380$ K for four different specimens. For these data the dark current is somewhat larger than the average photocurrent. An absolute agreement between the two measurements is obtained. This absolute agreement appears to be a conclusive demonstration that the assignment of t_R to recombination is valid. We found that if we used average photocurrents larger than the dark current that $\mu\tau_{ss}$ was smaller than $\mu\tau_{e,r}$, which is consistent with the commonly observed decline of $\mu\tau_{ss}$ with increasing illumination intensity in *a*-Si:H.[8,66,67]

B. Evaluation of $\mu\tau_{ss}$ and $\mu\tau_{e,t}$

At room temperature we were unable to estimate $\mu\tau_{e,r}$ from the transient photocharge under near dark conditions; t_R became longer than our experimental range of about 50 s. We estimate $\mu\tau_{ss}$ using quasi-steady-state illumination, although the average photocurrent greatly exceeded the dark current at room temperature. In Fig. 10 we correlate these room-temperature estimates of $\mu\tau_{ss}$ with the deep-trapping mobility-lifetime product $\mu\tau_{e,t}$ estimated using the transient photocharge method by evaluating $Q(t)(d^2/Q_0V)$ at 10 μs (i.e., after a deep-trapping time). The data suggest a proportionality

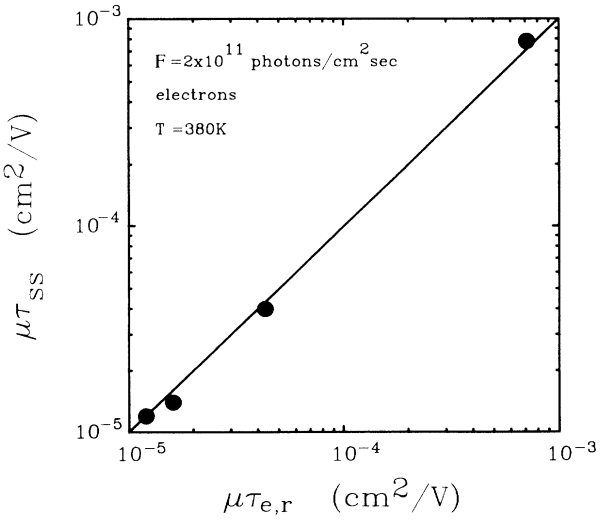

FIG. 9. Correlation of steady-state mobility-lifetime product $\mu\tau_{ss}$ and normalized transient photocharge $Q(t)(d^2/Q_0V)$ estimated at 10 s (after the recombination response time) for four *a*-Si:H specimens at 380 K. $\mu\tau_{ss}$ was estimated under the steady-state illumination flux of $F=2\times10^{11}$ photons/cm^2 s at 620 nm.

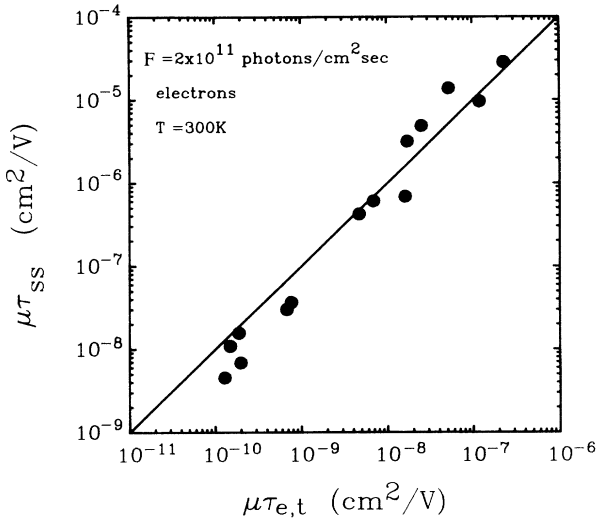

FIG. 10. Correlation of steady-state mobility-lifetime product $\mu\tau_{ss}$ and deep-trapping mobility-lifetime produce $\mu\tau_{e,t}$ for a variety of *a*-Si:H specimens at room temperature. The $\mu\tau_{ss}$ was estimated from steady-state photoconductivity under the illumination flux of $F=2\times10^{11}$ photons/cm^2 s at 620 nm. The $\mu\tau_{e,t}$ was estimated from normalized transient photocharge measurements estimated at 10 μs. A straight line has been drawn for $\mu\tau_{ss}=100\times\mu\tau_{e,t}$.

$\mu\tau_{ss}=100\times\mu\tau_{e,t}$ (under our particular average photon flux $F=2\times10^{11}$ photons/cm^2 s). For our specimens we found that $\mu\tau_{ss}\propto F^{-0.3}$;[36] $\mu\tau_{e,t}$ is not intensity dependent, since by definition it is measured in near-dark conditions.

This proportionality ($\mu\tau_{ss}=100\times\mu\tau_{e,t}$) is similar to that originally noted by Schiff[6] for *a*-Si:H and by Mackenzie and Paul[28] for *a*-$Si_{1-x}Ge_x$:H. In these earlier works the value of $\mu\tau_{e,t}$ was estimated using "charge collection" in diode structures (sandwich geometry) with strongly absorbed illumination; $\mu\tau_{ss}$ was estimated using standard coplanar photocurrent measurements. The data of Fig. 10 have the virtue that they establish this correlation using estimates of $\mu\tau_{e,t}$ and $\mu\tau_{ss}$ from exactly the same electrode structure and illumination wavelength. The fact that the same behavior is seen in the present work as in the earlier work based on charge-collection measurements is not particularly surprising; the equivalence of the present method for estimating $\mu\tau_{e,t}$ with the charge-collection technique has been established elsewhere.[35]

When the discrepancy between $\mu\tau_{e,t}$ and $\mu\tau_{ss}$ was first noted[6] it was not known exactly which instrumental differences between the two types of measurement accounted for it. We have shown that $\mu\tau_{ss}$ corresponds to the long-time value of $Q(t)(d^2/Q_0V)$, which we have denoted $\mu\tau_{e,r}$ (see also Ref. 5). The measurements of $Q(t)(d^2/Q_0V)$ presented in Sec. IV show conclusively that $\mu\tau_{e,t}$ and $\mu\tau_{e,r}$ correspond to completely different temporal regions, and that the ratio of the two quantities can be accounted for satisfactorily when the temporal effect is accounted for. Several other mechanisms have been proposed to account for the difference between $\mu\tau_{e,t}$ and $\mu\tau_{ss}$ including differences in illumination wavelength

TABLE III. Electron deep-trapping mobility-lifetime product $\mu\tau_{e,t}$, recombination mobility-lifetime product $\mu\tau_{e,r}$, and the ratio of these two for the specimens shown in Table II; the data were taken between 355 and 380 K.

Specimen	$\mu\tau_{e,t}$ (cm^2/V)	$\mu\tau_{e,r}$ (cm^2/V)	$\mu\tau_{e,r}/\mu\tau_{e,t}$
2	1.1×10^{-7}	9.0×10^{-5}	~900
3	3.0×10^{-8}	6.0×10^{-6}	200
5	9.1×10^{-8}	2.0×10^{-5}	220
6	3.1×10^{-7}	5.8×10^{-5}	185

and in specimen geometry.[6,29–32] These mechanisms clearly cannot account for the measurements presented here, where both $\mu\tau$ estimates were obtained under identical illumination conditions and in a single electrode structure.

In Table III we list the values of $\mu\tau_{e,t}$ and $\mu\tau_{e,r}$ as well as the ratio $\mu\tau_{e,r}/\mu\tau_{e,t}$ for the same specimens of Table II. Both $\mu\tau$ values correspond to temperatures between 356 and 380 K; recombination was observed at times earlier than 50 s. The ratio $\mu\tau_{e,r}/\mu\tau_{e,t}$ among three of the specimens is similar to 200 while for one of them is larger and close to 1000. We remind the reader that the $\mu\tau_{ss}/\mu\tau_{e,t}$ ratio—shown in Fig. 10—are smaller than the ratios shown in Table III, because of the sublinear dependence of $\mu\tau_{ss}$ upon the photon flux F.

We favor the following physical explanation for the large difference between the electron deep-trapping mobility-lifetime product $\mu\tau_{e,t}$ and steady-state mobility-lifetime product $\mu\tau_{ss}$: $\mu\tau_{e,t}$ corresponds to the drift of a photogenerated electron until its first "deep-trapping" event; recall that $\mu\tau$ products are essentially a proportionality factor between a drift length and the electric field. Deep trapping does not terminate electron drift; the electrons are subsequently reemitted, and in Sec. V we have analyzed this emission time. $\mu\tau_{ss}$ reflects the total drift of the electron including many-trapping and detrapping cycles, until recombination of the electron finally occurs.

The number of such trapping/detrapping cycles is determined by the recombination of electrons with holes. We would speculate that recombination corresponds to the process $e^- + D^+ \rightarrow D^0$, at least for the near-dark conditions emphasized in the present work.[68] In seems extraordinary that the ratio $\mu\tau_{ss}/\mu\tau_{e,t}$, is so well defined for specimens varying by orders of magnitude in deep-level density; there are two distinct published efforts to account for this phenomenon which we shall not review here.[9,69]

VII. EVOLUTION OF HOLES IN *a*-Si:H

We have not discussed the evolution of holes in this paper, although the subject is of greater significance for solar cells and other applications than electron evolution.[67] The early stages of hole evolution appear to be similar to those for electrons. In particular, holes are deep trapped, apparently by the same deep levels which deep trap electrons.[2,35] As for electrons, two important transport parameters can be estimated for holes: the deep-trapping mobility-lifetime product $\mu\tau_{h,t}$, and the ambipolar diffusion length,[70] which is usually attributed to the hole steady-state mobility-lifetime product $\mu\tau_{h,r}$. Surprisingly though, the correlation of the deep-trapping mobility-lifetime product with the steady-state one has never been done for holes.

We believe that published results support an empirical relation $\mu\tau_{h,r} \sim 100\times\mu\tau_{h,t}$, similar to the result just discussed for electrons. In general we estimate $\mu\tau_{h,t} \sim 10^{-3}\times\mu\tau_{ss}$, since $\mu\tau_{h,t} \sim 10^{-1}\times\mu\tau_{e,t}$ (Ref. 35) and $\mu\tau_{e,t} \sim 10^{-2}\times\mu\tau_{ss}$. A recent summary[8,67,71] of the correlation between $\mu\tau_{ss}$ and $\mu\tau_{h,r}$ estimated from the steady-state photoconductivity and steady-state photocarrier grating, respectively, suggests that $10^{-2}\times\mu\tau_{ss} < \mu\tau_{h,r} < 10^{-1}\times\mu\tau_{ss}$, from which we estimate that $10\times\mu\tau_{h,t} < \mu\tau_{h,r} < 10^2\times\mu\tau_{h,t}$. This inequality suggests reemission for holes after deep trapping, a situation very similar to that of electrons. However, this is a prediction and needs to be proven directly for the same specimen.

ACKNOWLEDGMENTS

The authors thank S. Hotaling, S. Zafar and J.-K. Lee for depositing and characterizing most of the specimens; also C. Nebel for useful discussions. This research was supported by the National Renewable Energy Laboratory through Subcontract No. XG-1-10063-7.

*Present address: Center for Photoinduced Charge Transfer, University of Rochester, Rochester, NY 14627-0166.

[1]T. Tiedje, in *Semiconductors and Semimetals,* edited by J. I. Pankove (Academic, New York, 1984), Vol. 21C, p. 207.

[2]R. A. Street, Philos. Mag. B **49**, L15 (1984), and references therein.

[3]S. P. Hotaling, Homer Antoniadis, and E. A. Schiff, Sol. Cells **27**, 357 (1989).

[4]S. P. Hotaling, Homer Antoniadis, and E. A. Schiff, J. Non-Cryst. Solids **114**, 420 (1989).

[5]Homer Antoniadis and E. A. Schiff, in *Amorphous Silicon Technolgoy,* edited by P. C. Taylor, M. J. Thompson, P. G. LeComber, Y. Hamakawa, and A. Madan, MRS Symposia Proceedings No. 192 (Materials Research Society, Pittsburgh, 1990), p. 293; J. Non-Cryst. Solids **137-138**, 435 (1991).

[6]E. A. Schiff, Philos. Mag. Lett. **55**, 87 (1987), and references therein.

[7]E. A. Schiff, M. A. Parker, and K. A. Conrad, in *Amorphous Silicon Technology,* edited by A. Madan, M. J. Thompson, P. C. Taylor, P. G. LeComber, and Y. Hamakawa, MRS Symposia Proceedings No. 118 (Materials Research Society, Pittsburgh, 1988), p. 477.

[8]J. Kočka, C. E. Nebel, and C. D. Abel, Philos. Mag. B **63**, 221 (1991).

[9]R. S. Crandall and I. Balberg, Appl. Phys. Lett. **58**, 508 (1991).

[10]J. M. Hvam and M. H. Brodsky, Phys. Rev. Lett. **46**, 371

(1981).
[11]C.-Y. Huang, S. Guha, and S. J. Hudgens, Phys. Rev. B **27**, 7460 (1983).
[12]R. Pandya, E. A. Schiff, and K. A. Conrad, J. Non-Cryst. Solids **66**, 193 (1983).
[13]P. Kirby and W. Paul, Phys. Rev. B **29**, 826 (1984).
[14]R. A. Street, Phys. Rev. B **32**, 3910 (1985).
[15]M. Kunst and A. Werner, J. Appl. Phys. **58**, 2236 (1985).
[16]H. Oheda, Philos. Mag. B **52**, 857 (1985).
[17]R. Pandya and E. A. Schiff, Philos. Mag. B **52**, 1075 (1985).
[18]K. A. Conrad and E. A. Schiff, Solid State Commun. **60**, 291 (1986).
[19]C. Main, R. Russel, J. Berkin, and J. M. Marshall, Philos. Mag. B **55**, 189 (1987).
[20]K. A. Conrad, Ph.D. thesis, Syracuse University, 1988.
[21]R. Könenkamp, S. Muramatsu, H. Itoh, S. Matsubara, and T. Shimada, Jpn. J. Appl. Phys. **29**, L2155 (1990).
[22]J. M. Marshall and C. Main, Philos. Mag. B **47**, 471 (1983).
[23]G. Le Saux and A. Brun, IEEE J. Quantum Electron. **QE-23**, 1680 (1987).
[24]E. A. Schiff, in *Tetrahedrally Bonded Amorphous Semiconductors,* edited by D. Adler and H. Fritzsche (Plenum, New York, 1985), p. 357.
[25]D. Melcher and E. A. Schiff (unpublished).
[26]W. Meyer and H. Neldel, Z. Phys. **12**, 588 (1937).
[27]H. Overhof and P. Thomas, in *Electronic Transport in Hydrogenated Amorphous Semiconductors,* Springer Tracts in Modern Phys. Vol. 114 (Springer, Berlin, 1989).
[28]K. D. Mackenzie and W. Paul, J. Non-Cryst. Solids **97-98**, 1055 (1987).
[29]M. A. Parker and E. A. Schiff, J. Non-Cryst. Solids **97-98**, 627 (1987).
[30]H. Kakinuma, Phys. Rev. B **39**, 10 473 (1989).
[31]M. Vaněček, J. Kočka, E. Šipek, and A. Třiska, J. Non-Cryst. Solids **114**, 447 (1989).
[32]C. Main, J. Berkin, R. Brüggemann, and J. M. Marshall, J. Non-Cryst. Solids **137-138**, 439 (1991).
[33]Von K. Hecht, Z. Phys. **77**, 235 (1932).
[34]R. A. Street, Appl. Phys. Lett. **41**, 1060 (1982).
[35]Homer Antoniadis and E. A., Schiff, Phys. Rev. B **44**, 3627 (1991).
[36]Homer Antoniadis, Ph.D. thesis, Syracuse University, 1992.
[37]F. Carasco and W. E. Spear, Philos. Mag. B **47**, 495 (1983).
[38]R. A. Street, J. Zesch, and M. J. Thompson, Appl. Phys. Lett. **43**, 672 (1983).
[39]J. M. Marshall, R. A. Street, and M. J. Thompson, Philos. Mag. B **54**, 51 (1986).
[40]R. Köenkamp, J. Non-Cryst. Solids **77-78**, 643 (1985).
[41]G. Schumm and G. H. Bauer, Phys. Rev. B **39**, 5311 (1989).
[42]J. P. Kleider, C. Longeaud and O. Glodt, J. Non-Cryst. Solids **137-138**, 447 (1991).
[43]K. Hattori, Y. Niwano, H. Okamoto, and Y. Hamakawa, J. Non-Cryst. Solids **137-138**, 363 (1991).
[44]R. Pandya and E. A. Schiff, J. Non-Cryst. Solids **59-60**, 297 (1983).
[45]C. Main, R. Brüggemann, D. P. Webb, and S. Reynolds, Solid State Commun. **83**, 401 (1992).
[46]P. G. LeComber and W. E. Spear, Philos. Mag. B **53**, L1 (1986), and references therein.
[47]K. L. Ngai and R. Q. Han, Solid State Commun. **68**, 155 (1988), and references therein.
[48]G. F. Seynhaeve, R. P. Bercley, G. J. Adriaenssens, and J. M. Marshall, Phys. Rev. B **39**, 10 196 (1989).
[49]D. S. Shen, J. P. Conde, V. Chu, J. Z. Liu, S. Aljishi, Z. Smith, A. Maruyama, and S. Wagner, Appl. Phys. Lett. **53**, 1542 (1988).
[50]R. Könenkamp, Phys. Rev. B **36**, 2938 (1987).
[51]D. Mendoza and W. Pickin, Phys. Rev. B **40**, 3914 (1989).
[52]T. M. Leen and J. D. Cohen, J. Non-Cryst. Solids **137-138**, 319 (1991), and references therein.
[53]R. S. Crandall, Phys. Rev. B **43**, 4057 (1991).
[54]W. B. Jackson, Phys. Rev. B **38**, 3595 (1988).
[55]R. Shinar, X.-L. Wu, S. Mitra, and J. Shinar, in *Amorphous Silicon Technology,* edited by A. Madan, M. J. Thompson, P. C. Taylor, P. G. LeComber, and Y. Hamakawa, MRS Symposia Proceedings No. 219 (Materials Research Society, Pittsburgh, 1991), p. 75.
[56]S. D. Brotherton and P. Bradley, J. Appl. Phys. **53**, 5720 (1982).
[57]A. Yelon and B. Movaghar, Phys. Rev. Lett. **65**, 618 (1990).
[58]K. Tanaka and H. Okushi, J. Non-Cryst. Solids **66**, 205 (1984).
[59]H. Okushi, Y. Tokumaru, S. Yamasaki, H. Oheda, and K. Tanaka, Phys. Rev. B **25** , 4313 (1982).
[60]K. L. Narasimhan and B. M. Arora, Solid State Commun. **55**, 615 (1985).
[61]V. Premachandran, K. L. Narasimhan, and D. R. Bapat, Phys. Rev. B **29**, 7073 (1984).
[62]C. R. Wronski, S. Lee, M. Hicks, and S. Kumar, Phys. Rev. Lett. **63**, 1420 (1989).
[63]S. Lee, D. Heller, and C. R. Wronski, in *Amorphous Silicon Technology,* edited by P. C. Taylor, M. J. Thompson, P. G. LeComber, Y. Hamakawa, and A. Madan, MRS Symposia Proceedings No. 192 (Materials Research Society, Pittsburgh, 1990), p. 89.
[64]G. D. Cody, T. Tiedje, B. Abeles, B. Brooks, and Y. Goldstein, Phys. Rev. Lett. **47**, 1480 (1981).
[65]G. Weiser and H. Mell, J. Non-Cryst. Solids **114**, 298 (1989).
[66]C. R. Wronski and R. E. Daniel, Phys. Rev. **23**, 794 (1981).
[67]E. A. Schiff, Sol. Cells **30**, 227 (1991), and references therein.
[68]E. A. Schiff, in *Disordered Semiconductors,* edited by M. A. Kastner, G. A. Thomas, and S. R. Ovshinsky (Plenum, New York, 1987), 379.
[69]J. Kočka, C. Nebel, and C. D. Abel, in *Proceedings of the Tenth European Conference on Photovoltaic Energy,* edited by A. Luque, G. Sala, W. Palz, G. Dos Santos, and P. Helm (Kluwer Academic, Dordrecht, 1991), p. 1091.
[70]D. Ritter, K. Weiser, and E. Zeldov, J. Appl. Phys. **62**, 4563 (1987), and references therein.
[71]F. Wang and R. Schwarz, J. Appl. Phys. **71**, 791 (1992), and references therein.

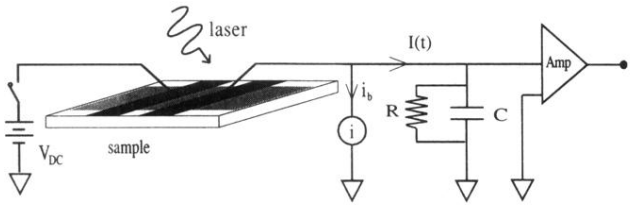

FIG. 3. Schematics for the transient photocharge measurements. The geometry of the substrate (Corning 7059) and of the coplanar electrodes evaporated onto the *a*-Si:H are shown. V_{DC} is the externally dc applied voltage; $I(t)$ is the transient photocurrent; i_b is the opposing steady-state current; C and R are the input capacitor and resistance, respectively.